

The nuclear moment of inertia and spin distribution of nuclear levels

Y. Alhassid,¹ G.F. Bertsch,² L. Fang,¹ and S. Liu¹

¹*Center for Theoretical Physics, Sloane Physics Laboratory,
Yale University, New Haven, CT 06520*

²*Department of Physics and Institute of Nuclear Theory, Box 351560
University of Washington Seattle, WA 98915*

We introduce a simple model to calculate the nuclear moment of inertia at finite temperature. This moment of inertia describes the spin distribution of nuclear levels in the framework of the spin-cutoff model. Our model is based on a deformed single-particle Hamiltonian with pairing interaction and takes into account fluctuations in the pairing gap. We derive a formula for the moment of inertia at finite temperature that generalizes the Belyaev formula for zero temperature. We show that a number-parity projection explains the strong odd-even effects observed in shell model Monte Carlo studies of the nuclear moment of inertia in the iron region.

PACS numbers: 21.60.-n, 21.60.Cs, 21.10.Hw, 05.30.-d

I. INTRODUCTION

The shell model Monte Carlo (SMMC) method has proven to be quite accurate for calculating the nuclear level density in the range of excitation energies up to several tens of MeV [1, 2, 3]. The advantage of the SMMC method is that it can be used to calculate thermal observables in model spaces that are orders of magnitude larger than can be treated by conventional diagonalization methods. In practice, most of the SMMC calculations are carried out in truncated spaces (e.g., one major shell), hence the limitation on the excitation energy. Correlations become less important at higher temperatures, and the results of the truncated SMMC calculations can be extended to higher temperatures or excitation energies by taking into account the effects of a larger space in the independent-particle model [4].

The SMMC method can also be used to calculate the distribution of nuclear spins at finite temperature [5]. However, this requires spin projection, and the associated computational effort is rather large. For general purposes such as constructing tables for large numbers of nuclei, simplified models are thus invaluable. The aim of this paper is to construct and study such a simple model that can reproduce well the spin distributions of the microscopic SMMC method.

A common assumption [6, 7] in global parameterizations of nuclear level densities is that the spin distribution follows the spin-cutoff model

$$\frac{\rho_J}{\rho} = \frac{2J+1}{2\sqrt{2\pi}\sigma^3} e^{-\frac{J(J+1)}{2\sigma^2}}. \quad (1)$$

Here ρ is the total level density counting all M states in a J multiplet, while ρ_J is the density of spin- J levels without the $2J+1$ degeneracy factor. Thus $\sum_J (2J+1)\rho_J = \rho$. The parameter σ is known as the spin cutoff parameter. The quantities ρ , ρ_J , and σ are all functions of excitation energy.

The model can be derived assuming that the individual nucleon spins add up as independent random vectors [8],

$\vec{J} = \sum_i \vec{J}_i$, leading to a Gaussian distribution of the spin vector $P(\vec{J}) \propto e^{-\vec{J}^2/2\sigma^2}$. Integrating over the orientation of \vec{J} , we have $P(J) \propto J^2 e^{-J^2/2\sigma^2}$, where J is the magnitude of the angular momentum (the pre-exponential factor J^2 comes from the Jacobian in spherical coordinates). We recover Eq. (1) by making the semiclassical substitution $J \rightarrow J + 1/2$; the spin cutoff parameter is then given by

$$\sigma^2 = \langle J_z^2 \rangle = \frac{1}{3} \langle \vec{J}^2 \rangle. \quad (2)$$

In thermal ensembles it is common to define an effective moment of inertia I by the relation between $\langle \vec{J}^2 \rangle$ and temperature T , which we can write as

$$I = \frac{\hbar^2}{T} \sigma^2. \quad (3)$$

In many of the empirical parameterizations, σ is determined by this formula using for I the rigid-body moment of inertia, $I = 2mA(r_0A^{1/3})^2/5$, where $r_0 \approx 1.2 - 1.3$ fm is the usual nuclear radius parameter, A is the mass number and m is the nucleon mass. Other treatments of σ based on the independent-particle model have also been proposed [9]. SMMC calculations of nuclei in the $A \sim 50 - 70$ mass region show that the assumption of a rigid-body moment of inertia breaks down at low excitation energies starting somewhat below the neutron separation energy, especially in even-even nuclei. The effect has a clear odd-even mass dependence. Furthermore, at the lowest excitations, deviations are observed from the spin-cutoff model itself, and odd-even staggering effects (in spin) can be seen. Here we will show that a fairly simple model based on a fixed deformation and a fluctuating pairing field reproduces very well the detailed SMMC results for the effective moment of inertia at finite temperature. In particular, odd-even effects observed in the microscopic SMMC calculations are nicely reproduced by a number-parity projection method [10, 11, 12, 13]. We would therefore advocate this model for global calculations of the spin distributions below the neutron separa-

tion energy. Such distributions are needed for theoretical estimates of nucleosynthesis reaction rates [7], among other applications.

Our model is based on the static path approximation [14, 15, 16] to the BCS Hamiltonian [17]. BCS theory is valid in the limit when the mean level spacing is much smaller than the pairing gap. However, this condition does not hold in the finite nucleus, in which case fluctuations must be taken into account. A similar situation occurs in ultra-small metallic particles whose linear size is smaller than ~ 3 nm [18]. Theoretical studies have indicated that pairing correlations in the crossover from BCS to the fluctuation-dominated regime are manifested through their number-parity dependence. Odd-even effects that originate in pairing correlations were found in the SMMC heat capacity of nuclei [19]. Such effects were also observed in the heat capacities of rare-earth nuclei that were extracted from level density measurements [20, 21]. Finite-temperature pairing correlations at a fixed number of particles were also studied in Ref. [22].

In this paper, we first discuss in Section II general aspects of calculating the thermal moment of inertia and projection on number parity. We work in a grand canonical ensemble, but the odd-even effects can be extracted by the number-parity projection operator. In Section III, we apply the formalism to a model Hamiltonian that includes a deformed single-particle field and a pairing interaction treated in the static path approximation. This yields a formula for the moment of inertia that is a generalization of the Belyaev formula [23] for zero temperature, explaining the suppression of the inertia at low temperature. In Section IV, we further generalize the moment-of-inertia formula to take into account odd-even differences, making use of the number-parity projection operator. In Section V, we apply the model to nuclei in the iron region using the $pf g_{9/2}$ shell with single-particle energies and wave functions determined from a deformed Woods-Saxon potential. The calculated moments of inertia are found to be in good agreement with the SMMC calculations.

II. FORMAL ASPECTS

In general, the SMMC method [24, 25] can be used to calculate thermal expectation values of observables \mathcal{O}

$$\langle \mathcal{O} \rangle = \frac{\text{Tr}(\mathcal{O}e^{-\beta H})}{Z}, \quad (4)$$

where

$$Z = \text{Tr}e^{-\beta H} \quad (5)$$

is the nuclear partition function. H is the nuclear Hamiltonian, containing rotational invariant one-body and two-body terms. In Ref. [24, 25] exact particle-number projection was performed to calculate the traces in Eq. (4) at fixed number of protons and neutrons.

In Ref. [5], the spin distribution was calculated using spin projection techniques. For temperatures that are not too low, it was found that the spin-cutoff model (1) describes rather well the spin distribution but with an energy-dependent moment of inertia. The purpose of the present work is to understand the temperature dependence of the moment of inertia in terms of a simple model. We note, however, that at the lowest temperatures the SMMC calculations reveal deviations from the spin-cutoff model (1), which are beyond the scope of the model discussed here.

A. Moment of inertia

In this work we shall assume that the spin distribution can be described by Eq. (1), and we therefore only need to calculate the variance σ^2 . The obvious way to do this is to evaluate the expectation value of the operator $\mathcal{O} = J^2$ directly from (4), as is done in SMMC. However, our model in Section III is based on a deformed Hamiltonian H_{def} , and for such Hamiltonians it is useful to define a moment of inertia tensor I_{ij} as the response of the nucleus to a rotational field $\vec{\omega}$.

We shall work in the grand-canonical ensemble, replacing H by $H' = H_{\text{def}} - \mu\hat{N}$ in Eqs. (5) and (4). In the presence of a rotational field, the Hamiltonian is given by $H' - \vec{\omega} \cdot \vec{J}$ and its free energy is

$$F(\beta, \vec{\omega}) = -\beta^{-1} \ln \text{Tr}e^{-\beta(H' - \vec{\omega} \cdot \vec{J})}. \quad (6)$$

The moment of inertia I_{ij} is defined by the expansion of F to second order in $\vec{\omega}$, $F(\beta, \vec{\omega}) = F(\beta, \omega = 0) - \frac{1}{2}I_{ij}\omega_i\omega_j$, where ω_i are the components of $\vec{\omega}$. Equivalently [26]

$$I_{ij} = -\frac{\partial^2 F}{\partial \omega_i \partial \omega_j} \Big|_{\omega=0} = \int_0^\beta d\tau \langle J_i(\tau) J_j(0) \rangle, \quad (7)$$

where

$$\langle J_i(\tau) J_j(0) \rangle = \frac{\text{Tr}[e^{-\beta H'} (e^{\tau H'} J_i e^{-\tau H'}) J_j]}{Z} \quad (8)$$

is the spin response function in imaginary time. For a rotationally invariant Hamiltonian, $J_i(\tau) = J_i$, and $I_{ij} = I\delta_{ij}$ with $I = \beta \langle J_z^2 \rangle = \beta \langle \vec{J}^2 \rangle / 3$, in agreement with Eqs. (2) and (3). Choosing the cranking axis along the fixed z -axis of the laboratory frame, we can calculate I from

$$I = \frac{\partial^2 F}{\partial \omega^2} \Big|_{\omega=0}, \quad (9)$$

where¹

$$F(\beta, \omega) = -T \ln \text{Tr}e^{-\beta(H' - \omega L_z)}, \quad (10)$$

¹ Here we use a different notation for the angular momentum in the laboratory frame to distinguish it from the angular momentum in the intrinsic frame.

and the angular momentum component along z is denoted by L_z .

A non-rotational invariant effective Hamiltonian arises in the mean-field approximation when the single-particle potential is deformed. In such a case H_{def} describes the Hamiltonian in the intrinsic frame of the nucleus. The quantity I_{ij} in Eq. (7) is then the moment of inertia tensor in this intrinsic frame, where J_i are the *intrinsic* components of the angular momentum \vec{J} . To recover the moment of inertia I in (3), it is necessary to integrate over all orientations of the intrinsic frame and then use (9). One obtains the result (see Appendix B)

$$I = \frac{1}{3}(I_{xx} + I_{yy} + I_{zz}). \quad (11)$$

Eq. (11) expresses the effective moment of inertia I in terms of the intrinsic principal moments I_{ii} .

B. Number-parity projection

The calculations in the previous Section II A were described in the grand-canonical ensemble. While this allows the average number of particles to be specified, it is not precise enough to reproduce odd-even effects. We note that the behavior of odd and even nuclei at low temperatures is quite different; the spin goes to zero for even nuclei due to pairing, but remains finite at zero temperature for odd nuclei. Exact particle-number projection can be done using the projection operator $P_N = \int_0^{2\pi} e^{i\phi(N-\hat{N})} d\phi / 2\pi$ as in the SMMC, but leads to cumbersome expressions. In order to capture the main odd-even effects, it is often sufficient to use a number-parity projection [10, 11, 12, 13] that distinguishes only between even and odd number of particles. The number-parity projection is defined by

$$P_\eta = \frac{1}{2} \left(1 + \eta e^{i\pi\hat{N}} \right), \quad (12)$$

where $\eta = 1$ or -1 describes the projection on an even or odd number of particles, respectively. Thus, the number-parity projected partition function is

$$Z_\eta = \text{Tr} \left(P_\eta e^{-\beta H'} \right) = \frac{1}{2} Z \left[1 + \eta \langle e^{i\pi\hat{N}} \rangle \right], \quad (13)$$

where the bracket denotes a thermal trace, $\langle \mathcal{O} \rangle \equiv \text{Tr} \left(\mathcal{O} e^{-\beta H'} \right) / \text{Tr} e^{-\beta H'}$. We can also calculate number-parity projected expectation values of observables

$$\langle \mathcal{O} \rangle_\eta \equiv \frac{\text{Tr} \left(\mathcal{O} P_\eta e^{-\beta H'} \right)}{\text{Tr} \left(P_\eta e^{-\beta H'} \right)}. \quad (14)$$

Using (12), we find

$$\langle \mathcal{O} \rangle_\eta = \frac{\langle \mathcal{O} \rangle + \eta \langle e^{i\pi\hat{N}} \rangle \langle \mathcal{O} \rangle_\pi}{1 + \eta \langle e^{i\pi\hat{N}} \rangle}, \quad (15)$$

where we have used the notation

$$\langle \mathcal{O} \rangle_\pi \equiv \frac{\text{Tr} \left(\mathcal{O} e^{i\pi\hat{N}} e^{-\beta H'} \right)}{\text{Tr} \left(e^{i\pi\hat{N}} e^{-\beta H'} \right)}. \quad (16)$$

The number-parity projected moment of inertia I_{ij}^η is defined from the second-order expansion (in $\vec{\omega}$) of the number-parity projected free energy

$$F_\eta = -T \ln \text{Tr} \left[P_\eta e^{-\beta(H' - \vec{\omega} \cdot \vec{J})} \right]. \quad (17)$$

We find

$$I_{ij}^\eta = \frac{\int_0^\beta d\tau \langle J_i(\tau) J_j(0) \rangle + \eta \langle e^{i\pi\hat{N}} \rangle \int_0^\beta d\tau \langle J_i(\tau) J_j(0) \rangle_\pi}{1 + \eta \langle e^{i\pi\hat{N}} \rangle}, \quad (18)$$

where $\langle J_i(\tau) J_j(0) \rangle_\pi$ is defined as in (16).

III. MODEL

We now ask, starting from the independent-particle shell model, what is the minimal model that will include the most relevant interaction effects for calculating the spin distribution. Clearly, the most important correlations are those associated with the quadrupole deformation and the pairing field. Both of these can be treated in a mean-field approximation, but the mean-field equations predict sharp transitions that are not supported by more detailed theories. Thus we go one step further in the finite-temperature theory, using the static path approximation (SPA) [14, 15, 16] of the partition function to include time-independent fluctuations of the order parameters.

We consider an Hamiltonian composed of an axially deformed Woods-Saxon well for the single-particle potential and orbital-independent pairing for the interaction. We denote by $|k\rangle$ the single-particle eigenstates in the deformed potential with energies ϵ_k . They can be divided into degenerate time-reversed pairs (k, \bar{k}) . For an axially symmetric potential, $|k\rangle = |q, \mu\rangle$ where μ is the projection of the angular momentum on the symmetry axis and q are other labels of the states. The time-reversed states are defined by $|\bar{k}\rangle = |q, -\mu\rangle = | -k \rangle$ (known as the BCS phase convention), and we adopt the convention $k > 0 \Leftrightarrow \mu > 0$. The Hamiltonian may then be expressed in the form

$$H_{\text{def}} = \sum_{k>0} \epsilon_k (a_k^\dagger a_k + a_{\bar{k}}^\dagger a_{\bar{k}}) - G P^\dagger P, \quad (19)$$

where P^\dagger is the pair creation operator, $P^\dagger = \sum_{k>0} a_k^\dagger a_{\bar{k}}^\dagger$, and G is the pairing strength.

A. Static path approximation

The Hamiltonian (19) contains a pairing interaction. Using the Hubbard-Stratonovich transformation,

the imaginary-time propagator $e^{-\beta H'}$ can be written as a functional integral over pairing fields of propagators that describe non-interacting quasi-particles. Here we shall use the SPA, which takes into account only time-independent pairing fields. The functional integral then reduces to an ordinary integral over a complex pairing field ξ [14]

$$e^{-\beta H'} \approx \frac{\beta G}{2\pi} \int d\xi d\xi^* e^{-\beta G|\xi|^2} e^{-\beta \sum_{k>0} H_k}, \quad (20)$$

where

$$H_k = (\epsilon_k - \mu - G/2)(a_k^\dagger a_k + a_{\bar{k}}^\dagger a_{\bar{k}}) - G\xi^* a_{\bar{k}} a_k - G\xi a_k^\dagger a_{\bar{k}}^\dagger + G/2. \quad (21)$$

Our model (19) describes nucleons moving in a deformed well, but it could have been derived from a rotationally invariant Hamiltonian that included quadrupolar two-body interaction. This would introduce five additional integration variables in the SPA integral (20), two representing the intrinsic deformation and three representing the orientation of the deformed field [16]. This integration over the Euler angles of the intrinsic frame is equivalent to the symmetry restoration described by (82).

1. Partition function

Using (20), we can represent the grand-canonical partition function in the form

$$Z = \frac{\beta G}{2\pi} \int d\xi d\xi^* e^{-\beta G|\xi|^2} \left(\prod_{k>0} \text{Tr}_k e^{-\beta H_k} \right). \quad (22)$$

Here we used $\text{Tr} \left(\prod_k e^{-\beta H_k} \right) = \prod_{k>0} \text{Tr}_k e^{-\beta H_k}$, where Tr_k is the trace evaluated in the Fock space of the orbital pair (k, \bar{k}) , i.e. in the 4-dimensional space spanned by $\{|n_k, n_{\bar{k}}\} = \{|0, 0\rangle, |0, 1\rangle, |1, 0\rangle, |1, 1\rangle\}$. In this representation, H_k is the matrix

$$H_k = \begin{pmatrix} G/2 & 0 & 0 & G\xi \\ 0 & \epsilon_k - \mu & 0 & 0 \\ 0 & 0 & \epsilon_k - \mu & 0 \\ G\xi^* & 0 & 0 & 2(\epsilon_k - \mu) - G/2 \end{pmatrix}. \quad (23)$$

The traces in (22) are easily evaluated by diagonalizing each H_k in the corresponding 4-dimensional space. The four eigenvalues are $\epsilon_k - \mu + \{-E_k, 0, 0, E_k\}$, where

$$E_k = \sqrt{(\epsilon_k - \mu - G/2)^2 + G^2|\xi|^2} \quad (24)$$

are the familiar quasiparticle energies² but now defined for an arbitrary complex pairing field ξ . The trace in the

subspace (k, \bar{k}) is then easily evaluated as

$$\begin{aligned} \text{Tr}_k e^{-\beta H_k} &= e^{-\beta(\epsilon_k - \mu)} 4 \cosh^2(\beta E_k/2) \\ &= e^{-\beta(\epsilon_k - \mu)} (1 + e^{-\beta E_k})(1 + e^{\beta E_k}). \end{aligned} \quad (25)$$

The last algebraic form is convenient when dividing by Z in the evaluation of expectation values, as the reciprocal is proportional to $f_k(1-f_k)$ where f_k are the quasiparticle occupation probabilities.

An alternative way of calculating the trace is to write $H_k = (\epsilon_k - \mu) + (a_k^\dagger a_{\bar{k}}) \mathcal{H}_k \begin{pmatrix} a_k \\ a_{\bar{k}}^\dagger \end{pmatrix}$ where \mathcal{H}_k is the 2×2 matrix

$$\mathcal{H}_k = \begin{pmatrix} \epsilon_k - \mu - \frac{G}{2} & G\xi \\ G\xi^* & -\epsilon_k + \mu + \frac{G}{2} \end{pmatrix}, \quad (26)$$

and use the identity [13]

$$\text{Tr} \exp \left[(a_k^\dagger a_{\bar{k}}) \mathcal{K} \begin{pmatrix} a_k \\ a_{\bar{k}}^\dagger \end{pmatrix} \right] = \det(1 + e^{\mathcal{K}}) \quad (27)$$

for the matrix $\mathcal{K} \equiv -\beta \mathcal{H}_k$. The eigenvalues of \mathcal{H}_k are just $\pm E_k$, leading again to Eq. (25).

The complete grand-canonical partition function is given by

$$Z = \frac{\beta G}{2\pi} \int d\xi d\xi^* e^{-\beta G|\xi|^2 - \beta \sum_{k>0} (\epsilon_k - \mu)} \prod_{k>0} 4 \cosh^2(\beta E_k/2). \quad (28)$$

It can also be written in the form

$$Z = \frac{\beta G}{2\pi} \int d\xi d\xi^* e^{-\beta F[\xi, \xi^*]}, \quad (29)$$

where

$$F[\xi, \xi^*] = G|\xi|^2 + \sum_{k>0} (\epsilon_k - \mu) - 2\beta^{-1} \sum_{k>0} \ln [2 \cosh(\beta E_k/2)] \quad (30)$$

is the free energy for a complex pairing field ξ .

The canonical partition function $Z_N = \text{Tr}_N e^{-\beta H}$ can be calculated by a Fourier transform of the grand-canonical partition

$$\begin{aligned} Z_N &= \frac{1}{2\pi i} \int_{-i\pi}^{i\pi} d\alpha e^{-\alpha N} \text{Tr}(e^{\alpha \hat{N}} e^{-\beta H}) \\ &= \frac{\beta G}{2\pi} \int d\xi d\xi^* \frac{1}{2\pi i} \int_{-i\pi}^{i\pi} d\alpha e^{-\alpha N} e^{-\beta F[\xi, \xi^*]}. \end{aligned} \quad (31)$$

The integrals in (31) can be evaluated in the saddle point approximation in both ξ and μ . The corresponding saddle-point equations, $\partial F/\partial \xi^* = 0$ and $\partial F/\partial \mu = -N$, will give the usual finite-temperature BCS equations

$$\frac{1}{G} = \sum_{k>0} \frac{\tanh\left(\frac{\beta E_k}{2}\right)}{2E_k}, \quad (32)$$

² One usually denotes the self-consistent $G|\xi|$ as Δ in BCS formulation.

and

$$N = \sum_{k>0} \left(1 - \frac{\epsilon_k - \mu - \frac{G}{2}}{E_k} \tanh \frac{\beta E_k}{2} \right), \quad (33)$$

where the quasi-particle energies E_k are given by (24). The solutions of (32) and (33) determine the pairing gap $\Delta = G|\xi|$ and the chemical potential μ as a function of T and particle number N (the phase of ξ is undetermined).

A better estimate of the canonical partition function Z_N can be obtained by a saddle-point integration in (31) over α for every ξ , but keeping the integration over ξ intact. We find

$$Z_N \approx 2\beta G \int_0^\infty d|\xi| |\xi| \left(2\pi T \frac{\partial^2 F}{\partial \mu^2} \right)^{-1/2} e^{-\beta(F[\xi, \xi^*] + \mu N)}, \quad (34)$$

where $\mu = \mu(N, T, \xi)$ is determined from $\partial F / \partial \mu = -N$, i.e., Eq. (33), and

$$\frac{\partial^2 F}{\partial \mu^2} = - \sum_{k>0} \frac{\beta E_k (\epsilon_k - \mu - \frac{G}{2})^2 + \sinh(\beta E_k) G^2 |\xi|^2}{2E_k^3 \cosh^2(\frac{\beta E_k}{2})}. \quad (35)$$

In Eq. (34) we have carried out explicitly the integral over the phase of the pairing field ξ since the integrand was only a function of $|\xi|$.

2. Moment of inertia

Our model (19) describes a non-rotationally invariant Hamiltonian, and we can use the formalism of Section II A to estimate the moment of inertia I in terms of the intrinsic moments I_{ii} (see Eq. (11)). Rather than using Eqs. (7) and (8) with the full Hamiltonian H , we first apply an SPA representation similar to (20) but for the cranked Hamiltonian in (6), and then calculate the intrinsic moments from $I_{ii} = \partial^2 F(\beta, \vec{\omega}) / \partial \omega_i^2 |_{\omega=0}$. If this is done starting from the canonical partition function in (6), we obtain the following expression

$$I_{ij} = \frac{\int d\xi d\xi^* \int_{-i\pi}^{i\pi} d\alpha e^{-\alpha N} e^{-\beta F[\xi, \xi^*]} \mathcal{I}_{ij}(\xi)}{\int d\xi d\xi^* \frac{1}{2\pi i} \int_{-i\pi}^{i\pi} d\alpha e^{-\alpha N} e^{-\beta F[\xi, \xi^*]}}, \quad (36)$$

where $F[\xi, \xi^*]$ is the free energy (30) and

$$\mathcal{I}_{ij}(\xi) = \int_0^\beta d\tau \text{Tr}[e^{-\beta H_\xi} J_i(\tau) J_j(0)] / \text{Tr}[e^{-\beta H_\xi}], \quad (37)$$

where $J_i(\tau) = e^{\tau H_\xi} J_i e^{-\tau H_\xi}$ and $H_\xi \equiv \sum_{k>0} H_k$ is the mean-field Hamiltonian in a pairing field ξ . Expression

(37) is analogous to (7) and (8), except that the Hamiltonian H' in those expressions is now replaced by H_ξ .

The integrals over α in (36) can be done in the saddle-point as before to obtain the final expression for the intrinsic moments

$$I_{ij} = \frac{\int_0^\infty d|\xi| |\xi| (\partial^2 F / \partial \mu^2)^{-1/2} e^{-\beta(F[\xi, \xi^*] + \mu N)} \mathcal{I}_{ij}(\xi)}{\int_0^\infty d|\xi| |\xi| (\partial^2 F / \partial \mu^2)^{-1/2} e^{-\beta(F[\xi, \xi^*] + \mu N)}}. \quad (38)$$

It remains to calculate the moments $\mathcal{I}_{ij}(\xi)$. The operator J_z leaves the (k, \bar{k}) subspace invariant, but the operators J_x and J_y connect different subspaces k and k' , so the trace in (37) is to be evaluated in a 16-dimensional space. This is most conveniently done in the quasiparticle representation. The transformation from deformed single-particle states to the quasi-particle states is achieved through a Bogoliubov transformation

$$\begin{pmatrix} \alpha_k \\ \alpha_{\bar{k}}^\dagger \end{pmatrix} = U_k \begin{pmatrix} a_k \\ a_{\bar{k}}^\dagger \end{pmatrix} = \begin{pmatrix} u_k & -v_k \\ v_k^* & u_k \end{pmatrix} \begin{pmatrix} a_k \\ a_{\bar{k}}^\dagger \end{pmatrix}, \quad (39)$$

where u_k is real and v_k is complex, and $u_k^2 + |v_k|^2 = 1$ to preserve the fermionic commutation relations. Relations (39) imply

$$u_{\bar{k}} = u_k; \quad v_{\bar{k}} = -v_k \quad \text{for } k > 0. \quad (40)$$

The parameters u_k, v_k are chosen such that H_k in Eq. (21) is diagonal in the quasi-particle representation, i.e.,

$$U_k^\dagger \mathcal{H}_k U_k = \begin{pmatrix} E_k & 0 \\ 0 & -E_k \end{pmatrix}, \quad (41)$$

where \mathcal{H}_k is the 2×2 matrix (26) and E_k are the eigenvalues (24) of \mathcal{H}_k . The solution is

$$u_k^2 = \frac{1}{2} \left(1 + \frac{\epsilon_k - \mu - G/2}{E_k} \right) \quad (42)$$

$$|v_k|^2 = \frac{1}{2} \left(1 - \frac{\epsilon_k - \mu - G/2}{E_k} \right),$$

and $\arg v_k = \arg \xi$. The Hamiltonian H_k is now given by $H_k = (\epsilon_k - \mu) + E_k(\alpha_k^\dagger \alpha_k - \alpha_{\bar{k}} \alpha_{\bar{k}}^\dagger)$, and

$$H_\xi = \sum_{k>0} E_k (\alpha_k^\dagger \alpha_k + \alpha_{\bar{k}}^\dagger \alpha_{\bar{k}}) + \sum_{k>0} (\epsilon_k - \mu - E_k). \quad (43)$$

Expressing J_i in the quasi-particle representation, and using (43), we can calculate the intrinsic moments in closed form (see Appendix A). The final result is

$$\mathcal{I}_{ij}(\xi) = \sum_{k,l>0} [(\langle k|j_i|l\rangle\langle k|j_j|l\rangle^* + \langle k|j_i|l\rangle\langle k|j_j|l\rangle^*) + c.c.] \left\{ (u_k u_l + v_k v_l)^2 \frac{f_l - f_k}{E_k - E_l} + (u_k v_l - v_k u_l)^2 \frac{1 - f_k - f_l}{E_k + E_l} \right\}, \quad (44)$$

where

$$f_k = \frac{1}{1 + e^{\beta E_k}} \quad (45)$$

are the quasi-particle occupations. u_k and v_k are still given by (42), except that now we have chosen

$$u_k, v_k > 0 \quad \text{for } k > 0, \quad (46)$$

and $u_{\bar{k}}, v_{\bar{k}}$ are still given by (40). Eq. (44) is the finite-temperature generalization of the Belyaev formula [23].

Eq. (44) can be rewritten by separating out the contribution from the $k = l$ terms in the sum. Using $(f_l - f_k)/(E_k - E_l) \xrightarrow{k=l} -\partial f_k / \partial E_k$, we obtain (for $i = j$)

$$\begin{aligned} \mathcal{I}_{ii}(\xi) = & 2 \sum_{k>0} (|\langle k|j_i|k\rangle|^2 + |\langle k|j_i|k\rangle|^2) \left(-\frac{\partial f_k}{\partial E_k} \right) + 2 \sum_{k,l>0} (|\langle k|j_i|l\rangle|^2 + |\langle k|j_i|l\rangle|^2) \\ & \times \left\{ (u_k u_l + v_k v_l)^2 \frac{f_l - f_k}{E_k - E_l} + (u_k v_l - v_k u_l)^2 \frac{1 - f_k - f_l}{E_k + E_l} \right\}. \end{aligned} \quad (47)$$

In particular, $\langle k|j_z|l\rangle = 0$ for $k \neq l$, and $\langle k|j_x|k\rangle = 0$. Therefore, the moment of inertia around an axis parallel to the symmetry axis z (non-collective rotation) is given by

$$\mathcal{I}_{zz}(\xi) = 2 \sum_{k>0} |\langle k|j_z|k\rangle|^2 \left(-\frac{\partial f_k}{\partial E_k} \right), \quad (48)$$

while the moment of inertia around an axis x perpendicular to the symmetry axis (collective rotation) is given by

$$\begin{aligned} \mathcal{I}_{xx}(\xi) = & 2 \sum_{k>0} |\langle k|j_x|k\rangle|^2 \left(-\frac{\partial f_k}{\partial E_k} \right) + 2 \sum_{k,l>0} (|\langle k|j_x|l\rangle|^2 + |\langle k|j_x|l\rangle|^2) \\ & \times \left\{ (u_k u_l + v_k v_l)^2 \frac{f_l - f_k}{E_k - E_l} + (u_k v_l - v_k u_l)^2 \frac{1 - f_k - f_l}{E_k + E_l} \right\}. \end{aligned} \quad (49)$$

In the limit $T \rightarrow 0$ (but $\Delta > 0$), $-\partial f_k / \partial E_k \rightarrow \delta(E_k)$, and since $E_k > 0$, $\mathcal{I}_{zz}(\xi) = 0$. Also $f_k \rightarrow 0$ and Eq. (49) reduces to

$$I_{xx}(\xi) = 2 \sum_{k \neq l > 0} (|\langle k|j_x|l\rangle|^2 + |\langle k|j_x|l\rangle|^2) \frac{(u_k v_l - v_k u_l)^2}{E_k + E_l} = \sum_{k,l} |\langle k|j_x|l\rangle|^2 \frac{(u_k v_l - v_k u_l)^2}{E_k + E_l}. \quad (50)$$

Eq. (50) is known as the Belyaev formula [23]; it produces a moment of inertia that is suppressed relative to the rigid-body value.

IV. NUMBER-PARITY PROJECTION

In the relations we derived in the previous Section for the partition function and moment of inertia, the number of particles is fixed only on average, and odd-even effects cannot be reproduced. Here we go through the same derivation steps but include now the number-parity projection operator P_η . The resulting formulas will exhibit explicit terms depending on the number parity.

A. Partition function

The projected partition function (13) introduces the operator $e^{i\pi \hat{N}}$. In the SPA

$$\begin{aligned} \text{Tr} \left(e^{i\pi \hat{N}} e^{-\beta H'} \right) &= \frac{\beta G}{2\pi} \int d\xi d\xi^* e^{-\beta G |\xi|^2} \\ &\times \prod_{k>0} \text{Tr}_k \left[e^{i\pi (a_k^\dagger a_k + a_{\bar{k}}^\dagger a_{\bar{k}})} e^{-\beta H_k} \right]. \end{aligned} \quad (51)$$

Within each subspace (k, \bar{k}) , the operator $e^{i\pi \hat{N}}$ changes the sign of the two vectors $|0, 1\rangle, |1, 0\rangle$, but leaves the sign of $|0, 0\rangle, |1, 1\rangle$ unchanged. The matrix representing

$e^{i\pi(a_k^\dagger a_k + a_k^\dagger a_{\bar{k}})}$ is then

$$\begin{pmatrix} 1 & 0 & 0 & 0 \\ 0 & -1 & 0 & 0 \\ 0 & 0 & -1 & 0 \\ 0 & 0 & 0 & 1 \end{pmatrix}. \quad (52)$$

The transformation that diagonalizes H_k in Eq. (23) leaves this matrix invariant, and therefore the trace is now given by

$$\begin{aligned} \text{Tr}_k \left[e^{i\pi(a_k^\dagger a_k + a_k^\dagger a_{\bar{k}})} e^{-\beta H_k} \right] &= e^{-\beta(\epsilon_k - \mu)} 4 \sinh^2(\beta E_k / 2) \\ &= e^{-\beta(\epsilon_k - \mu)} (1 - e^{-\beta E_k}) (e^{\beta E_k} - 1). \end{aligned} \quad (53)$$

The projected grand-canonical partition function $Z_\eta \equiv \text{Tr} \left(P_\eta e^{-\beta H'} \right)$ is now calculated from (25) and (53) to be

$$Z_\eta = \frac{\beta G}{4\pi} \int d\xi d\xi^* e^{-\beta F[\xi, \xi^*]} \left(1 + \eta \prod_{k>0} \tanh^2 \frac{\beta E_k}{2} \right). \quad (54)$$

Notice that the integrand in (54) has the form of Eq. (13) when applied to the Hamiltonian $H_\xi = \sum_{k>0} H_k$ at a fixed pairing field ξ . Indeed

$$\langle e^{i\pi \hat{N}} \rangle_\xi \equiv \frac{\text{Tr} \left(e^{i\pi \hat{N}} e^{-\beta H_\xi} \right)}{\text{Tr} e^{-\beta H_\xi}} = \prod_{k>0} \tanh^2 \frac{\beta E_k}{2}. \quad (55)$$

This projected partition can also be written as $Z_\eta = \frac{\beta G}{2\pi} \int d\xi d\xi^* e^{-\beta F_\eta[\xi, \xi^*]}$ where

$$F_\eta[\xi, \xi^*] = F[\xi, \xi^*] - \beta^{-1} \ln \left(\frac{1 + \eta \prod_{k>0} \tanh^2 \frac{\beta E_k}{2}}{2} \right) \quad (56)$$

is the number-parity projected free energy. Proceeding as in Section III A 1, we can derive (in the saddle point approximation) number-parity projected BCS equations

$$\frac{1}{G} = \sum_{k>0} \left(\frac{\tanh \left(\frac{\beta E_k}{2} \right)}{2E_k} + \frac{C_\eta}{E_k \sinh(\beta E_k)} \right), \quad (57)$$

and

$$N = \sum_{k>0} \left[1 - \frac{\epsilon_k - \mu - \frac{G}{2}}{E_k} \left(\tanh \frac{\beta E_k}{2} + \frac{2C_\eta}{\sinh(\beta E_k)} \right) \right], \quad (58)$$

where

$$C_\eta = \frac{\eta \prod_{k>0} \tanh^2 \left(\frac{\beta E_k}{2} \right)}{1 + \eta \prod_{k>0} \tanh^2 \left(\frac{\beta E_k}{2} \right)}. \quad (59)$$

It is interesting to take the $T \rightarrow 0$ limit for the above equations. For $\eta = +1$, they simply become the usual $T = 0$ BCS equations. However, for the odd projection

$\eta = -1$, we find (assuming there are no degeneracies and $\Delta = G|\xi| > 0$)

$$\begin{aligned} \frac{1}{G} &= \sum_{k>0} \frac{1}{2E_k} - \frac{1}{2E_{k_0}} \\ N &= \sum_{k \neq k_0 > 0} 2|v_k|^2 + 1, \end{aligned} \quad (60)$$

where $|v_k|^2$ is given by (42) and E_{k_0} is the lowest quasi-particle energy (corresponding to ϵ_{k_0} closest to μ). In deriving (60), we have used the limit $C_{-1} \xrightarrow{\beta \rightarrow \infty} -e^{\beta E_{k_0}}/4$. Eqs. (60) reproduce what is known as the blocking effect, since one level $k = k_0$ is ‘‘blocked’’ and does not contribute to the sum over k .

In Fig. 1 we display the solution of the number-parity projected BCS equations for a Hamiltonian corresponding to the nucleus ^{56}Fe . The pairing gap Δ is shown as the solid line as a function of temperature T . For the particle-number projected BCS equations (57), the solutions for even and odd particle numbers are shown as the dot-dashed and dashed lines, respectively. The proton gap Δ_p and the neutron gap Δ_n are shown in the left and right panels. Note the strong suppression of the gap for the odd projection. Our results for the projected gap are qualitatively similar to Ref. [12, 13], but the formulas are quite different.

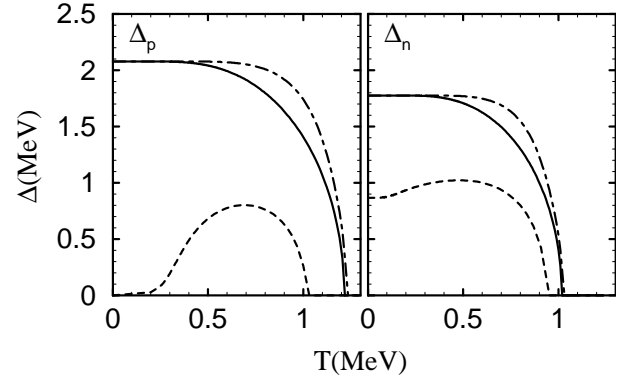


FIG. 1: The pairing gap Δ versus temperature T for protons (left) and neutrons (right). The solid lines are the solution of the BCS equations (32) for ^{56}Fe . The dotted-dashed lines and the dashed lines are respectively the solution to the number-parity projected BCS equations (57) for $\eta = 1$ and $\eta = -1$. The deformation parameter is taken to be $\beta_2 = 0.24$ and the pairing strengths are determined from the zero-temperature BCS to reproduce the experimental values of the gaps (using the second difference formula of Ref. [27]).

The number-parity projected partition function at a fixed average number of particles is given by an equation similar to (34) except that F is replaced by F_η .

B. Moment of inertia

The number-parity projected moment of inertia can be calculated as in Section III A 2, but now starting from the number-parity projected free energy in the presence of a rotational field $\vec{\omega}$. The result is

$$I_{ij}^\eta = \frac{\int_0^\infty d|\xi| |\xi| (\partial^2 F_\eta / \partial \mu^2)^{-1/2} e^{-\beta(F_\eta[\xi, \xi^*] + \mu N)} \mathcal{I}_{ij}^\eta(\xi)}{\int_0^\infty d|\xi| |\xi| (\partial^2 F_\eta / \partial \mu^2)^{-1/2} e^{-\beta(F_\eta[\xi, \xi^*] + \mu N)}}, \quad (61)$$

where

$$I_{ij}^\eta(\xi) = \int_0^\beta d\tau \frac{\text{Tr} [P_\eta e^{-\beta H_\xi} J_i(\tau) J_j(0)]}{\text{Tr} [P_\eta e^{-\beta H_\xi}]}. \quad (62)$$

For the intrinsic moment of inertia we find

$$\mathcal{I}_{ij}^\eta(\xi) = \frac{\int_0^\beta d\tau \langle J_i(\tau) J_j(0) \rangle + \eta \prod_{k>0} \tanh^2 \frac{\beta E_k}{2} \int_0^\beta d\tau \langle J_i(\tau) J_j(0) \rangle_\pi}{1 + \eta \prod_{k>0} \tanh^2 \frac{\beta E_k}{2}}, \quad (64)$$

where $\int_0^\beta d\tau \langle J_i(\tau) J_j(0) \rangle$ is given by (44) and $\int_0^\beta d\tau \langle J_i(\tau) J_j(0) \rangle_\pi$ is obtained from the expression for $\int_0^\beta d\tau \langle J_i(\tau) J_j(0) \rangle$ by the substitution

$$f_k \rightarrow \tilde{f}_k = \frac{1}{1 - e^{\beta E_k}}. \quad (65)$$

We now inspect the $T \rightarrow 0$ limit of Eq. (64). For the even number-parity projected inertia $\mathcal{I}_{zz}^{\eta=1} \rightarrow 0$ and $\mathcal{I}_{xx}^{\eta=1}$ is the same as in Eq. (50). For the odd number-parity projected moment of inertia, we have in the limit $T \rightarrow 0$

$$\mathcal{I}_{zz}^{\eta=-1} \rightarrow \beta |\mu_0|^2, \quad (66)$$

where $|k_0\rangle = |q, \mu_0\rangle$ (E_{k_0} is the lowest quasi-particle energy), and

$$\begin{aligned} \mathcal{I}_{xx}^{\eta=-1} \rightarrow & 2 \sum_{k \neq k_0 > 0} (|\langle k | j_x | k_0 \rangle|^2 + |\langle k | j_x | -k_0 \rangle|^2) \left\{ \frac{(u_k u_{k_0} + v_k v_{k_0})^2}{E_k - E_{k_0}} + \frac{(u_k v_{k_0} - v_k u_{k_0})^2}{E_k + E_{k_0}} \right\} \\ & + 2 \sum_{k, l \neq k_0 > 0} (|\langle k | j_x | l \rangle|^2 + |\langle k | j_x | -l \rangle|^2) \frac{(u_k v_l - v_k u_l)^2}{E_k + E_l} + \beta |\langle k_0 | j_x | -k_0 \rangle|^2. \end{aligned} \quad (67)$$

The number-parity projected moments of inertia I_{ij}^η are computed by a numerical integration of Eq. (61), using Eq. (44) and (64). For the final result, the contributions from the three principal axes must be combined according to Eq. (11).

V. COMPARISON TO SMMC RESULTS

We have used our formulas to study the moment of inertia I versus temperature for nuclei in the iron region and compared the results with SMMC calculations. The effective Hamiltonian is defined in the full $pf g_{9/2}$ shell with single-particle energies determined by a Woods-Saxon potential plus spin-orbit term. The interaction includes $T = 1$ monopole pairing and multipole-multipole

Thus we need to calculate the projected value $\langle J_i(\tau) J_j(0) \rangle_\eta$. The odd-even number projection can be carried out for any operator \mathcal{O} using (15) at a fixed pairing field ξ together with (55)

$$\langle \mathcal{O} \rangle_\eta = \frac{\langle \mathcal{O} \rangle + \eta \left(\prod_{k>0} \tanh^2 \frac{\beta E_k}{2} \right) \langle \mathcal{O} \rangle_\pi}{1 + \eta \left(\prod_{k>0} \tanh^2 \frac{\beta E_k}{2} \right)}. \quad (63)$$

In general, $\langle \mathcal{O} \rangle_\pi = \text{Tr} \left(\mathcal{O} e^{i\pi \hat{N}} e^{-\beta H_\xi} \right) / \text{Tr} \left(e^{i\pi \hat{N}} e^{-\beta H_\xi} \right)$ will have the same form as $\langle \mathcal{O} \rangle$ but with $e^{\pm \beta E_k}$ replaced by $-e^{\pm \beta E_k}$.

interaction terms (up to hexadecupole) [1]. In SMMC we calculate $\langle J_z^2 \rangle$ as an observable and then find I from

$$\frac{I}{\hbar^2} = \beta \langle J_z^2 \rangle. \quad (68)$$

Significant odd-even effects are observed in the SMMC calculations [5], see, e.g., in Fig. 2 where the SMMC thermal moment of inertia of the even-even nucleus ^{56}Fe (solid circles) is compared with the SMMC moment of inertia of the odd-even nucleus ^{55}Fe (open circles). We see stronger suppression at the lower temperatures in the even-even case.

The parameters of the model we discuss in the present work are the deformation β_2 and the pairing strengths G_p, G_n for protons and neutrons, respectively. We have chosen $\beta_2 = 0.14$ and computed G_p and G_n from the experimental values of Δ_p and Δ_n (using zero-temperature

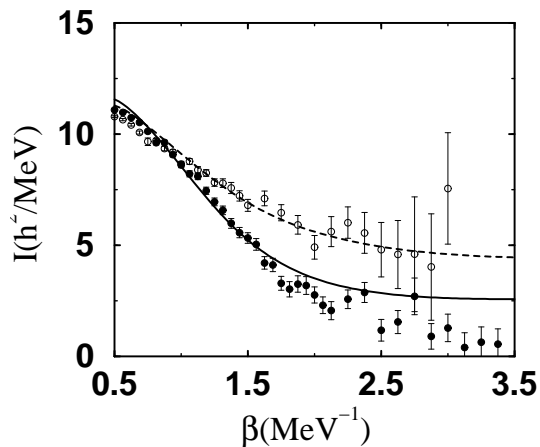


FIG. 2: Moment of inertia (characterizing the spin-cutoff distribution (1)) versus inverse temperature β for an even-even nucleus (^{56}Fe) and an odd-even nucleus (^{55}Fe). The SMMC results calculated from (68) are shown by the solid circles for ^{56}Fe and the open circles for ^{55}Fe . The results of the model discussed in this work (which includes fluctuations of the pairing field and number-parity projection) are shown by solid line for ^{56}Fe and dashed line for ^{55}Fe . For protons we use even number-parity projection, while for neutrons we use even (odd) number-parity projection for ^{56}Fe (^{55}Fe). In the model we use a deformation of $\beta_2 = 0.14$ and pairing strengths of $G_p = 0.42$ and $G_n = 0.36$.

BCS). In our model, we include fluctuations in the pairing gap and we have found it necessary to reduce the BCS values of G by about 20% to reproduce correctly the high temperature behavior of I . We then fixed $\beta_2 = 0.14$, $G_p = 0.42$ and $G_n = 0.36$ through the whole mass region, and calculated the number-parity projected moment of inertia I^η (with fluctuations in the pairing order parameter included) using Eqs. (11), (61), (64) and (44). Fig. 2 shows the results for I^η in ^{56}Fe (solid line) and in ^{55}Fe (dashed line). We find that the inclusion of a number parity projection allows us describe reasonably well the odd-even effect observed in the SMMC moment of inertia. We note that an exact particle-number projection (for both protons and neutrons) is used in the SMMC method.

To demonstrate the importance of fluctuations in the pairing order parameter, we show in Fig. 3 the number-parity projected moments of inertia $I^\eta(\xi)$ evaluated at the corresponding solutions ξ to the number-parity projected BCS equations (57) but without the inclusion of fluctuations. $I^\eta(\xi)$ is calculated from (64) and averaging over principal axes. We use the same deformation and pairing parameters as in the theory with fluctuations. These results demonstrate that we cannot obtain good agreement with the microscopic SMMC calculations without including fluctuations.

In Fig. 4 we present a systematic study of the moment of inertia for even and odd iron isotopes from ^{55}Fe to

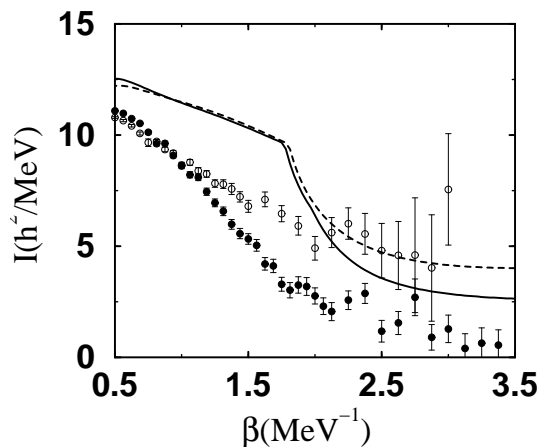


FIG. 3: Similar to Fig. 2 but the lines correspond to the number-parity projected moments of inertia calculated at the solutions ξ of the corresponding number-parity BCS equations (57). The deformation and pairing parameters are the same as in Fig. 2.

^{60}Fe . We show the moment of inertia versus β , comparing the SMMC results (symbols with statistical error bars) to our model results (solid lines for even isotopes and dashed lines for odd isotopes). The model includes fluctuations in the pairing fields, and we have used a fixed set of deformation and pairing parameters. Despite its simplicity, the results of our model agree well with the full microscopic SMMC calculation.

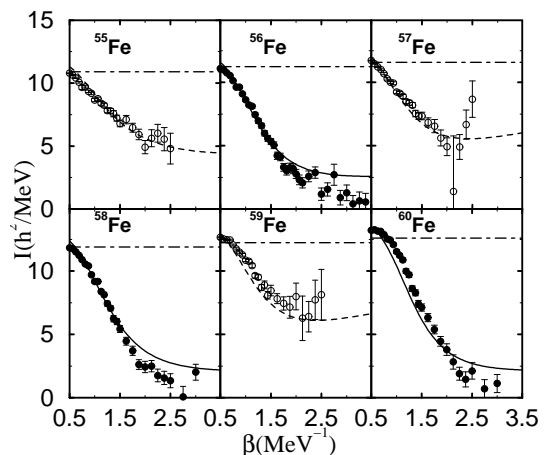


FIG. 4: Systematics of the moment of inertia versus β for a series of iron isotopes. The symbols (solid circles for even-mass isotopes and open circles for odd-mass isotopes) are the SMMC results calculated from (68). The lines describe the results of our model (including fluctuations in the pairing field). The solid lines are the even number-parity projection while the dashed lines describe the odd number-parity projection. The dotted-dashed lines are the rigid-body moment of inertia. We use $\beta_2 = 0.14$ and $G_p = 0.42$, $G_n = 0.36$.

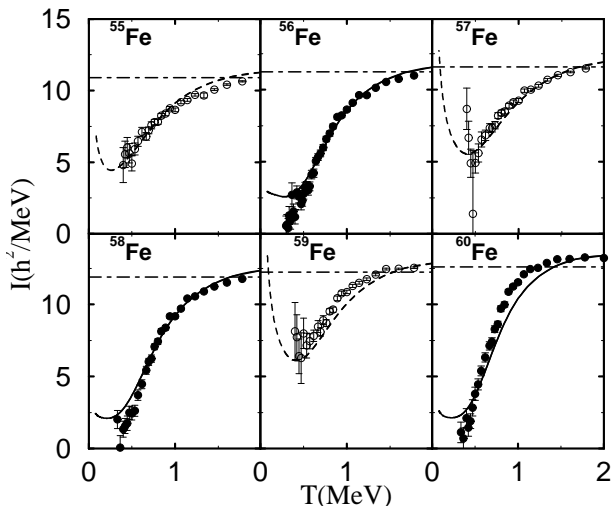


FIG. 5: As in Fig. 4, except that the moments of inertia are shown versus temperature.

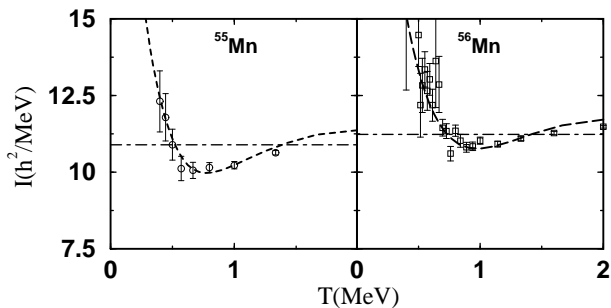


FIG. 6: The moments of inertia versus temperature for the odd-even nucleus ^{55}Mn and the odd-odd nucleus ^{56}Mn . The notation as in Fig. 4.

In Fig. 5 we show the same results as in Fig. 4 but plotted as a function of temperature. In general, the thermal moment of inertia is seen to decrease with decreasing temperature with stronger suppression in the even isotopes. Furthermore, for the odd iron isotopes (in which an odd number-parity projection is used for neutrons), the moment of inertia starts to rise at low temperatures. Indeed, according to (68)

$$I \rightarrow \frac{1}{3}\beta J(J+1), \quad (69)$$

for large β where J is the ground-state spin. In an odd-even nucleus, $J \neq 0$ and I increases linearly with β at large β . In the model this rise at low temperatures can be understood to be the effect of the unpaired neutron. Using the projected moment of inertia for odd number of particles, we find in the limit of large β

$$I^{\eta=-1} \rightarrow \frac{1}{3}\beta(\mu_0^2 + |\langle k_0 | j_x | -k_0 \rangle|^2), \quad (70)$$

where the second term in (70) contributes only for $\mu_0 = 1/2$. It is interesting to note that a similar odd-even effect was found in the spin susceptibility of ultra-small metallic particles (nanoparticles) [28]. The rise of the spin susceptibility at low temperatures for an odd number of electrons is known as re-entrant behavior and survives in the fluctuation-dominated regime.

Finally, in Fig. 6 we show the moment of inertia versus temperature for an odd-even nucleus ^{55}Mn (left panel) and for an odd-odd nucleus ^{56}Mn (right panel). We have used the same deformation and pairing strength parameters as for the iron nuclei. Again we find good agreement between the results of the model (dashed lines) and the microscopic SMMC calculations (symbols).

VI. CONCLUSION

We have presented a simple model to calculate the nuclear moment of inertia at finite temperature. The model includes quadrupolar deformation of the single-particle field and pairing interaction. The pairing interaction is treated beyond the mean-field BCS limit by including static fluctuations in the pairing order parameter at finite temperature.

In the fluctuation-dominated regime, finite temperature signatures of pairing correlations are often observed as odd-even effects (in particle number) [18]. Such signatures are usually not seen in the grand-canonical ensemble, but only after particle-number projection is implemented (such as in SMMC). In this work we have used number-parity projection instead of exact particle-number projection and showed that the odd-even effects in the moment of inertia seen in the microscopic SMMC calculations can be well reproduced. The advantage of such number-parity projection is its simplicity, which allows us to express the projected moment of inertia in essentially closed form (except for an integral over the pairing field).

The simple model developed here is useful in estimating the spin distribution of nuclear level densities at not-too-low temperatures for which the spin-cutoff model usually works well. The spin-cutoff model depends on a single parameter – the moment of inertia, and thus our model is useful for global estimates of the spin distribution below the neutron separation energy where the moment of inertia may deviate from its rigid-body value.

Acknowledgment

We thank R. Vandenbosch for discussions. Y.A. would like to acknowledge the hospitality of the Institute of Nuclear Theory in Seattle where part of this work was completed. This work is supported by the DOE under Grants DE-FG-02-91ER40608 and DE-FGO3-00ER41132.

Appendix A: finite-temperature generalization of the Belyaev formula for the moment of inertia tensor

Here we derive Eq. (44). Since H_ξ is diagonal in the quasi-particle representation (see Eq. (43)), we have

$$\begin{aligned}\alpha_k^\dagger(\tau) &\equiv e^{\tau H_\xi} \alpha_k^\dagger e^{-\tau H_\xi} = e^{\tau E_k} \alpha_k^\dagger \\ \alpha_k(\tau) &\equiv e^{\tau H_\xi} \alpha_k e^{-\tau H_\xi} = e^{-\tau E_k} \alpha_k.\end{aligned}\quad (71)$$

Using (71) and the Bogoliubov transformation (39), we obtain

$$\begin{aligned}J_i(\tau) &= \sum_{k,l} \langle k|j_i|l \rangle a_k^\dagger(\tau) a_l(\tau) = \sum_{k,l} \langle k|j_i|l \rangle (u_k \alpha_k^\dagger(\tau) + v_k \alpha_{\bar{k}}(\tau)) (u_l \alpha_l(\tau) + v_l \alpha_l^\dagger(\tau)) \\ &= \sum_{k,l} \langle k|j_i|l \rangle \left[e^{\tau(E_k - E_l)} u_k u_l \alpha_k^\dagger \alpha_l + e^{\tau(E_l - E_k)} v_k v_l \alpha_{\bar{k}} \alpha_l^\dagger + e^{\tau(E_k + E_l)} u_k v_l \alpha_k^\dagger \alpha_l^\dagger + e^{-\tau(E_k + E_l)} v_k u_l \alpha_{\bar{k}} \alpha_l \right].\end{aligned}\quad (72)$$

The spin response function is then given by

$$\begin{aligned}\langle J_i(\tau) J_j(0) \rangle &= \sum_{k,l,m,n} \langle k|j_i|l \rangle \langle m|j_j|n \rangle \times \left[e^{\tau(E_k - E_l)} u_k u_l u_m u_n \langle \alpha_k^\dagger \alpha_l \alpha_m^\dagger \alpha_n \rangle + e^{-\tau(E_k - E_l)} v_k v_l u_m u_n \langle \alpha_{\bar{k}} \alpha_l^\dagger \alpha_m^\dagger \alpha_n \rangle \right. \\ &\quad + e^{\tau(E_k - E_l)} u_k u_l v_m v_n \langle \alpha_k^\dagger \alpha_l \alpha_{\bar{m}} \alpha_n^\dagger \rangle + e^{-\tau(E_k - E_l)} v_k v_l v_m v_n \langle \alpha_{\bar{k}} \alpha_l^\dagger \alpha_{\bar{m}} \alpha_n^\dagger \rangle \\ &\quad \left. + e^{\tau(E_k + E_l)} u_k v_l v_m u_n \langle \alpha_k^\dagger \alpha_l^\dagger \alpha_{\bar{m}} \alpha_n \rangle + e^{-\tau(E_k + E_l)} v_k u_l u_m v_n \langle \alpha_{\bar{k}} \alpha_l \alpha_m^\dagger \alpha_n^\dagger \rangle \right].\end{aligned}\quad (73)$$

Using Wick's theorem in the quasi-particle representation and $f_k = f_{\bar{k}}$, we find

$$\begin{aligned}\langle J_i(\tau) J_j(0) \rangle &= \sum_k \{ \langle k|j_i|k \rangle [u_k^2 f_k + v_k^2 (1 - f_k)] \} \times \sum_m \{ \langle m|j_j|m \rangle [u_m^2 f_m + v_m^2 (1 - f_m)] \} \\ &\quad + \sum_{k,l} \langle k|j_i|l \rangle \langle l|j_j|k \rangle \times \left[e^{\tau(E_k - E_l)} u_k^2 u_l^2 f_k (1 - f_l) + e^{-\tau(E_k - E_l)} v_k^2 v_l^2 (1 - f_k) f_l \right. \\ &\quad \left. + e^{\tau(E_k + E_l)} u_k^2 v_l^2 f_k f_l + e^{-\tau(E_k + E_l)} v_k^2 u_l^2 (1 - f_k) (1 - f_l) \right] \\ &\quad + \sum_{k,l} \langle k|j_i|l \rangle \langle \bar{k}|j_j|\bar{l} \rangle \times u_k v_k u_l v_l \left[-e^{\tau(E_k - E_l)} f_k (1 - f_l) - e^{-\tau(E_k - E_l)} (1 - f_k) f_l \right. \\ &\quad \left. + e^{\tau(E_k + E_l)} f_k f_l + e^{-\tau(E_k + E_l)} (1 - f_k) (1 - f_l) \right].\end{aligned}\quad (74)$$

The sum in the first term is zero by symmetry (we assume axially symmetric deformed states). To proceed, we need to carefully examine the behavior of the matrix elements of j_i under time reversal. Denoting by \mathcal{T} the time reversal operator (cf. Ref. [27], 1-2c), we have $\mathcal{T} j_i \mathcal{T}^{-1} = -j_i$, and for $k > 0$ (i.e., for spin projection $\mu > 0$)

$$\begin{aligned}\mathcal{T}|k\rangle &= \mathcal{T}|q, \mu\rangle = |q, -\mu\rangle = |\bar{k}\rangle \\ \mathcal{T}|-k\rangle &= \mathcal{T}|q, -\mu\rangle = -|q, \mu\rangle = -|k\rangle.\end{aligned}\quad (76)$$

Using the transformation properties of the matrix elements under time reversal [see (1-34) in [27]], we then have

$$\begin{aligned}\langle k|j_i|l \rangle &= -\langle \bar{l}|j_i|\bar{k} \rangle \text{ for } k \cdot l > 0 \\ \langle k|j_i|l \rangle &= \langle \bar{l}|j_i|\bar{k} \rangle \text{ for } k \cdot l < 0.\end{aligned}\quad (77)$$

Using relations (77), we can rewrite (74) in the form

$$\langle J_i(\tau) J_j(0) \rangle = \sum_{k,l>0} (\langle k|j_i|l \rangle \langle l|j_j|k \rangle + \langle l|j_i|k \rangle \langle k|j_j|l \rangle + \langle k|j_i|-l \rangle \langle -l|j_j|k \rangle + \langle -k|j_i|l \rangle \langle l|j_j|-k \rangle) \quad (78)$$

$$\times \left[e^{\tau(E_k - E_l)} (u_k^2 u_l^2 + u_k v_k u_l v_l) f_k (1 - f_l) + e^{-\tau(E_k - E_l)} (v_k^2 v_l^2 + u_k v_k u_l v_l) (1 - f_k) f_l \right] \quad (79)$$

$$+ e^{\tau(E_k + E_l)} (u_k^2 v_l^2 - u_k v_k u_l v_l) f_k f_l + e^{-\tau(E_k + E_l)} (v_k^2 u_l^2 - u_k v_k u_l v_l) (1 - f_k) (1 - f_l) \quad (80)$$

The intrinsic moments are given by $\mathcal{I}_{ij} = \int_0^\beta d\tau \langle J_i(\tau) J_j(0) \rangle$. Using (78) and the relations

$$\begin{aligned}f_k (1 - f_l) \int_0^\beta e^{\tau(E_k - E_l)} d\tau &= (1 - f_k) f_l \int_0^\beta e^{-\tau(E_k - E_l)} d\tau = \frac{f_l - f_k}{E_k - E_l} \\ f_k f_l \int_0^\beta e^{-\tau(E_k + E_l)} d\tau &= (1 - f_k) (1 - f_l) \int_0^\beta e^{\tau(E_k + E_l)} d\tau = \frac{1 - f_k - f_l}{E_k + E_l},\end{aligned}\quad (81)$$

we arrive at Eq. (44).

Appendix B: derivation of the effective moment of inertia

Here we derive Eq. (11). The components L_μ of the angular momentum in the laboratory frame are related to the components J_i in the intrinsic frame through $L_\mu = \sum_{\mu'} \mathcal{D}_{\mu\mu'}^{(1)*}(\psi, \theta, \phi) J_{\mu'}$, where $\mathcal{D}^{(1)}$ are Wigner rotation matrices and (ψ, θ, ϕ) are Euler angles. In particular $L_z = \sum_i \hat{\omega}_i J_i$ where the unit vector $\hat{\omega}$ is given by $\hat{\omega} = (-\sin\theta \cos\phi, \sin\theta \sin\phi, \cos\theta)$. To restore rotational invariance, we integrate over all the possible orientations of the intrinsic frame. In practice we replace in (10)

$$e^{-\beta(H' - \omega L_z)} \rightarrow \frac{1}{4\pi} \int_0^{2\pi} d\phi \int_0^\pi d\theta \sin\theta e^{-\beta(H' - \omega \sum_i \hat{\omega}_i J_i)}, \quad (82)$$

and use (9) to find

$$I = \frac{1}{4\pi} \int_0^{2\pi} d\phi \int_0^\pi d\theta \sin\theta \sum_{ij} \hat{\omega}_i I_{ij} \hat{\omega}_j. \quad (83)$$

where I_{ij} is the intrinsic moment of inertia tensor (8). The explicit integration of (83) leads to (11).

-
- [1] H. Nakada and Y. Alhassid, Phys. Rev. Lett. **79**, 2939 (1997).
 - [2] Y. Alhassid, S. Liu, and H. Nakada, Phys. Rev. Lett. **83**, 4265 (1999).
 - [3] Y. Alhassid, G.F. Bertsch, S. Liu and H. Nakada, Phys. Rev. Lett. **84** (2000).
 - [4] Y. Alhassid, G.F. Bertsch, and L. Fang, Phys. Rev. C **68**, 044322 (2003).
 - [5] Y. Alhassid, S. Liu, and H. Nakada, to be published.
 - [6] A.S. Iljinov, M.V. Mebel, N. Bianchi, E. Desanctis, C. Guaraldo, V. Lucherini, V. Muccifora, E. Polli, A.R. Reolon, and P. Rossi, Nucl. Phys. A **543**, 517 (1992).
 - [7] T. Rauscher, F. Thielemann, and K. Kratz, Phys. Rev. C **56**, 1613 (1997).
 - [8] T. Ericson, Adv. Phys. **9**, 425 (1960).
 - [9] S. Goriely, Nucl. Phys. A **605**, 28 (1996).
 - [10] A.L. Goodman, Nucl. Phys. A **352**, 30 (1981).
 - [11] R. Rossignoli, N. Canosa and P. Ring, Phys. Rev. Lett. **80**, 1853 (1998).
 - [12] R. Balian, H. Flocard, and M. Veneroni, Phys. Rep. **317**, 252 (1999).
 - [13] H. Flocard, in "Atomic Clusters and Nanoparticles," ed. C. Guet, (Springer, Heidelberg, 2001), p. 271.
 - [14] B. Muhlschlegel, D.J. Scalapino and R. Denton, Phys. Rev. B **6**, 1767 (1972).
 - [15] Y. Alhassid and J. Zingman, Phys. Rev. C **30**, 684 (1984).
 - [16] B. Lauritzen, P. Arve and G.F. Bertsch, Phys. Rev. Lett. **61**, 2835 (1988).
 - [17] J. Bardeen, L.N. Cooper and J.R. Schrieffer, Phys. Rev. **108**, 1175 (1957).
 - [18] J. von Delft and D.C. Ralph, *Phys. Rep.* **345**, 61 (2001).
 - [19] S. Liu and Y. Alhassid, Phys. Rev. Lett. **87**, 022501 (2001).
 - [20] A. Schiller, A. Bjerve, M. Guttormsen, M. Hjorth-Jensen, F. Ingelbretsen, E. Melby, S. Messelt, J. Rekstad, S. Siem, and S.W. Odegard, Phys. Rev. C **63**, 021306 (R) (2001).
 - [21] M. Guttormsen, A. Bagheri, R. Chankova, J. Rekstad, S. Siem, A. Schiller, and A. Voinov, Phys. Rev. C **68**, 064306 (2003).
 - [22] S. Frauendorf, N.K. Kuzmenko, V.M. Mikhajlov, and J.A. Sheikh, Phys. Rev. B **68**, 024518 (2003).
 - [23] S.T. Belyaev, Nucl. Phys. **24**, 322 (1961).
 - [24] G. H. Lang, C. W. Johnson, S. E. Koonin and W. E. Ormand, Phys. Rev. **C48**, 1518 (1993).
 - [25] Y. Alhassid, D. J. Dean, S. E. Koonin, G. H. Lang, and W. E. Ormand, Phys. Rev. Lett. **72**, 613 (1994).
 - [26] Y. Alhassid, S. Levit and J. Zingman, Nucl. Phys. A **469**, 205 (1987).
 - [27] A. Bohr and B.R. Mottelson, *Nuclear Structure*, vol. 1 (Benjamin, New York, 1969).
 - [28] A. Di Lorenzo, R. Fazio, F.W.J. Hekking, G. Falci, A. Mastellone, and G. Giaquinta, Phys. Rev. Lett. **84**, 550 (2000).